Available online at www.sciencedirect.com
ScienceDirect
Journal of Computational Physics 222 (2007) 9–27
JOURNAL OF COMPUTATIONAL PHYSICS
www.elsevier.com/locate/jcp

Analysis of iterated ADI-FDTD schemes for Maxwell curl equations

B.D. Welfert

Department of Mathematics and Statistics, Arizona State University, Tempe, AZ 85287-1804, United States

Received 11 October 2005; received in revised form 3 May 2006; accepted 9 May 2006
Available online 22 November 2006

Abstract

The convergence of the iterative ADI-FDTD method proposed by Wang et al. [S. Wang, F. Teixeira, J. Chen, An iterative ADI-FDTD with reduced splitting error, IEEE Microwave Wireless Comp. Lett. 15 (2005) 1531–1533] towards the classical implicit Crank–Nicolson scheme when applied to Maxwell curl equations, and the accuracy, stability, and dispersion properties of the resulting iterated schemes are investigated. The iterated schemes are shown both mathematically and numerically to be unconditionally stable for 2D wave problems, in agreement with numerical experiments conducted in [S. Wang, F. Teixeira, J. Chen, An iterative ADI-FDTD with reduced splitting error, IEEE Microwave Wireless Comp. Lett. 15 (2005) 1531–1533]. However these schemes lose their unconditional stability when applied to full 3D wave problems where TE and TM modes do not decouple, as illustrated by numerical experiments in a PEC box.

Keywords: Finite difference time domain; Alternate direction implicit scheme; Fixed-point iteration; Iterated scheme; von Neumann stability; Unconditional stability; Dispersion relation

1. Introduction

The alternating-direct ion-implicit (ADI) finite-difference-time-domain method [26,12] is a popular scheme for solving the three-dimensional Maxwell curl equations. The ADI scheme is a compromise between standard explicit schemes such as the popular Yee scheme [21], which is efficient but unstable for larger time steps (due to CFL restrictions), and fully implicit schemes such as Crank–Nicolson (CN), which is unconditionally stable but inefficient (a 3D system must be solved at each time-step). On the other hand, the ADI scheme combines efficiency (requiring the solution of one-dimensional systems only at each time-step), with unconditional stability, and has been successfully applied to a variety of wave propagation and scattering problems, in particular in low frequency bioelectromagnetics.

Both CN and ADI schemes are second-order accurate (in the classical, non-stiff, sense) in time and in space. However, the ADI scheme lacks isotropy in dispersion properties and has been observed to have inferior

E-mail address: welfert@asu.edu.
URL: http://math.asu.edu/~bdw.

0021-9991/$ - see front matter © 2006 Published by Elsevier Inc.
doi:10.1016/j.jcp.2006.05.038

accuracy, compared to the CN scheme, in regions with large field gradients, e.g. around singularities associated with corners or near-field sources [8].

A variety of modifications of the ADI scheme designed to circumvent these problems have recently emerged.

- Richardson extrapolation and deferred correction ideas were considered in [10,6] to improve the accuracy in the ADI solution. The extrapolation method combines two second-order ADI solutions obtained with different step sizes into a single fourth-order approximation, while the deferred correction method uses an estimate of the local truncation error of the ADI scheme, obtained from a standard ADI solution, as an explicit source term in a second ADI run. These ideas can be iterated to provide additional accuracy, although successive extrapolations/corrections may have an undesirable effect on stability [10].
- Efforts to correct the ADI solution "on the fly", i.e., at the time-step level, include ideas based on extrapolation [1], symmetrization [20], and iterative correction [19]. Numerical results provided in the references seem to indicate that these strategies may be beneficial in improving the accuracy. However none of them considers the effect of modifications on stability, and numerical experiments only address two-dimensional TE or TM wave applications.

In this study we examine, both analytically and numerically, the iterative correction approach introduced in [19]. This approach defines a sequence of iterated ADI schemes using a fixed point (FP) iteration on the CN equations preconditioned with ADI. The resulting iterated schemes were tested in [19] on a two-dimensional TE wave only (an unspecified extrapolated version was mentioned). Further experiments on TE wave problems with a variable number of fixed-point iterations according to local spatial requirements were conducted in [18]. In particular, we investigate: (a) the convergence of the fixed-point iteration towards the CN scheme; and (b) the accuracy, stability and dispersion properties of the iterated schemes obtained for a fixed number of fixed-point iterations.

In Section 2 we set up the Maxwell curl system in Fourier space used in the subsequent accuracy and stability analysis. Known accuracy, stability and dispersion properties of the CN, ADI, and the Yee schemes [21] are summarized in Section 3. The iterated schemes are analyzed in Section 4. We show that the sequence of iterated schemes does converge to the CN scheme, that each scheme resulting from a fixed number of fixed-point iterations is unconditionally stable when applied to two-dimensional TE or TM wave problems (as in the numerical experiments conducted in [18,19]), but are unstable when applied to full three-dimensional wave problems with coupled TE and TM modes, even at low CFL numbers. Our conclusions are supported by a complete Fourier analysis of the 2D case, as well as numerical experiments in a three dimensional PEC box, reported in Section 5.

2. Maxwell system in Fourier space

We consider the (scaled) 3D Maxwell system

$$\partial_t u = \mathscr{A} u + \mathscr{B} u \tag{1}$$

in free space, where $u = [E,H]^{\mathrm{T}}$ and

$$\mathcal{A} = \left[\begin{array}{ccc|ccc} & & & 0 & 0 & \partial_y \\ & & & \partial_z & 0 & 0 \\ & & & 0 & \partial_x & 0 \\ \hline 0 & \partial_z & 0 & & & \\ 0 & 0 & \partial_x & & & \\ \partial_y & 0 & 0 & & & \end{array}\right], \quad \mathcal{B} = \left[\begin{array}{ccc|ccc} & & & 0 & -\partial_z & 0 \\ & & & 0 & 0 & -\partial_x \\ & & & -\partial_y & 0 & 0 \\ \hline 0 & 0 & -\partial_y & & & \\ -\partial_z & 0 & 0 & & & \\ 0 & -\partial_x & 0 & & & \end{array}\right]. \tag{2}$$

For a plane wave

$$u(t,x,y,z) \to \hat{u}(t)\mathrm{e}^{-\mathrm{j}(k_x x+k_y y+k_z z)} \quad (\mathrm{j}^2=-1)$$

with wave numbers (k_x,k_y,k_z), the system (1) becomes

$$\frac{\mathrm{d}\hat{u}}{\mathrm{d}t} = A\hat{u} + B\hat{u}, \tag{3}$$

where A and B are 6×6 matrices obtained by replacing the spatial derivatives ∂_α in $\mathscr{A}$ and $\mathscr{B}$ by

$$\partial_\alpha \to -\mathrm{j}k_\alpha \quad (\alpha = x,y,z), \tag{4}$$

where ($\hat{u}$ represents the spatial Fourier transform of u). Upon spatial discretization of (1) one only gets an approximation of $\mathrm{j}k_\alpha$. For example, second-order central difference FDTD approximations based on staggered grids for E and H, as in the Yee scheme [21], leads to the substitution

$$\partial_\alpha \to -\mathrm{j}\tilde{k}_\alpha, \quad \tilde{k}_\alpha = k_\alpha f\left(\frac{k_\alpha \Delta\alpha}{2}\right) \quad (\alpha = x,y,z) \tag{5}$$

with

$$f(\phi) = \frac{\sin\phi}{\phi} \tag{6}$$

on a uniform grid with spacing $\Delta\alpha$ in the α-direction. Since $|f(\phi)| \leqslant 1$, we have

$$|\tilde{k}_\alpha| \leqslant |k_\alpha|, \tag{7}$$

i.e., one effect of spatial discretization is to lower the exact wave number (leading to aliasing for higher wave numbers on a fixed grid). This effect becomes less pronounced as the grid is refined, or if higher-order spatial stencils are used, e.g. fourth-order explicit differentiation ($f(\phi) = \frac{\sin\phi}{\phi}(1+\frac{1}{6}\sin^2\phi)$ [17,22]) or implicit differentiation ($f(\phi) = \frac{\sin\phi}{\phi}\frac{12}{11+\cos 2\phi}$, [7,23]), see also [13] for a collection of schemes and references.

3. CN and ADI schemes

We are interested in comparing (the stability properties of) the CN and ADI schemes with constant step size Δt applied to the ordinary differential system (3). For simplicity we shall make the following substitutions:

$$\hat{u} \to u, \quad \frac{1}{2}\Delta t A \to A, \quad \frac{1}{2}\Delta t B \to B \tag{8a}$$

and let

$$\frac{1}{2}\Delta t\tilde{k}_\alpha = W_\alpha \tag{8b}$$

(compare [2,25,26]). For f defined by (6) the inequality

$$|W_\alpha| \leqslant \frac{\Delta t}{\Delta\alpha} \tag{9}$$

yields

$$W = \sqrt{W_x^2+W_y^2+W_x^2} \leqslant \Delta t\sqrt{\frac{1}{(\Delta x)^2}+\frac{1}{(\Delta y)^2}+\frac{1}{(\Delta z)^2}} \equiv \mathrm{CFL} \tag{10}$$

for any $\Delta\alpha$ ($\alpha = x,y,z$). Near equality in (9) occurs for wave numbers $|k_\alpha| \approx \frac{\pi}{\Delta\alpha}$, corresponding to modes which are not well resolved on the finite difference grid.

Upon the substitutions (8) the matrices A and B become

$$A = -j\left[\begin{array}{ccc|ccc} & & & 0 & 0 & W_y \\ & & & W_z & 0 & 0 \\ & & & 0 & W_x & 0 \\ \hline 0 & W_z & 0 & & & \\ 0 & 0 & W_x & & & \\ W_y & 0 & 0 & & & \end{array}\right], \quad B = j\left[\begin{array}{ccc|ccc} & & & 0 & W_z & 0 \\ & & & 0 & 0 & W_x \\ & & & W_y & 0 & 0 \\ \hline 0 & 0 & W_y & & & \\ W_z & 0 & 0 & & & \\ 0 & W_x & 0 & & & \end{array}\right],$$

respectively.

The CN scheme defines an approximation u^{n+1} of u at time $(n+1)\Delta t$ as

$$(I - A - B)u^{n+1} = (I + A + B)u^n. \tag{11}$$

This iteration requires the solution of a 6×6 linear system with matrix $I - A - B$. Adding ABu^{n+1} on each side of (11) and factoring yields

$$(I - A)(I - B)u^{n+1} = (I + A)(I + B)u^n + AB(u^{n+1} - u^n). \tag{12}$$

The ADI scheme defines u^{n+1} as

$$(I - A)(I - B)u^{n+1} = (I + A)(I + B)u^n \tag{13}$$

which can be obtained by dropping the last term in (12) [8]. The ADI scheme is normally implemented in split form

$$(I - A)u^{n+\frac{1}{2}} = (I + B)u^n, \tag{14a}$$

$$(I - B)u^{n+1} = (I + A)u^{n+\frac{1}{2}} \tag{14b}$$

(note that $I - A$ and $I + A$ commute), which requires the solution of two 6×6 systems with matrices $I - A$ sand $I - B$, both of which can both be permuted into block diagonal matrices with 2×2 diagonal blocks, and can therefore be easily inverted [9,12,26].

3.1. Stability/dispersion

The iteration matrices

$$T_{\mathrm{CN}} = (I - A - B)^{-1}(I + A + B)$$

of (11) and

$$T_{\mathrm{ADI}} = (I - B)^{-1}(I - A)^{-1}(I + A)(I + B) \tag{15}$$

of (13) both have double eigenvalues

$$\lambda = 1,\ \mathrm{e}^{2\mathrm{j}\theta},\ \mathrm{e}^{-2\mathrm{j}\theta} \tag{16}$$

with

$$\tan\theta_{\mathrm{CN}} = \sqrt{W_x^2 + W_y^2 + W_z^2} = W \tag{17}$$

for CN and

$$\tan\theta_{\mathrm{ADI}} = \sqrt{\frac{W_x^2 + W_y^2 + W_z^2 + W_x^2W_y^2 + W_y^2W_z^2 + W_z^2W_x^2}{1 + W_x^2W_y^2W_z^2}} \tag{18}$$

for ADI (compare [3,25]). Using the trigonometric identity $\cos^2\theta = (1 + \tan^2\theta)^{-1}$ one obtains, for a 2D $\mathrm{TE}_z/\mathrm{TM}_z$ wave ($W_z = 0$), the relation

$$\cos\theta_{\mathrm{ADI}} = \cos\theta_{\mathrm{CN}}\sqrt{1-\rho} \tag{19}$$

with

$$\rho = \frac{W_x^2 W_y^2}{(1+W_x^2)(1+W_y^2)}. \tag{20}$$

In comparison, the exact flow of the semi-discretized problem (3) has iteration matrix

$$T_{\mathrm{exact}} = \mathrm{e}^{2(A+B)} \tag{21}$$

with eigenvalues of the form (16), where

$$\theta_{\mathrm{exact}} = \sqrt{W_x^2 + W_y^2 + W_z^2} = W. \tag{22}$$

For reference, the standard Yee scheme [21]

$$(I-U)u^{n+1} = (I+L)u^n, \tag{23}$$

where

$$U = 2j\left[\begin{array}{c|ccc} & 0 & W_z & -W_y \\ & -W_z & 0 & W_x \\ & W_y & -W_x & 0 \\ \hline & & & \end{array}\right], \quad L = 2(A+B) - U,$$

corresponds to a Gauss–Seidel waveform relaxation with iteration matrix

$$T_{\mathrm{Yee}} = (I-U)^{-1}(I+L).$$

The eigenvalues of T_{Yee} are of the form (16) with

$$\sin\theta_{\mathrm{Yee}} = \sqrt{W_x^2 + W_y^2 + W_z^2} = W \tag{24}$$

provided $W \leqslant 1$, which, in view of (10), is guaranteed for CFL $\leqslant 1$.

The fact that $|\lambda_{\mathrm{ADI}}| = 1$ uniformly for all (W_x, W_y, W_z) (i.e., all (k_x, k_y, k_z)) is not sufficient in itself to guarantee unconditional stability because the Von Neumann criterion does not apply to multiple eigenvalues (a counter-example can be found in [11]). Although one can argue that the double eigenvalues of the ADI iteration matrix are in fact associated to independent TE and TM modes, unconditional stability of the ADI scheme is best shown by interpreting T_{ADI} as a composition of two unitary transformations [3], or via an energy estimate in the spirit of [4], see also [5] and Appendix A.

Fig. 1, left, displays the dispersion relation between θ and θ_{exact} for the CN and ADI schemes, using a discrete set of (W_x, W_y, W_z) triplets. The relation between θ_{CN} and θ_{exact} is one-to-one, namely, $\tan\theta_{\mathrm{CN}} = \theta_{\mathrm{exact}}$. On the other hand, the relation between θ_{ADI} and θ_{exact} is not one-to-one, but depends on the direction of the wave. This situation corresponds to the case $\Delta\alpha \to 0$ associated to the semi-discretized problem $(k_\alpha = \tilde{k}_\alpha)$.

To visualize the effect of spatial discretization we replace θ_{exact} in (22) by its limit

$$\lim_{\Delta\alpha\to 0}\theta_{\mathrm{exact}} = \frac{\Delta t}{2}k, \quad k = \sqrt{k_x^2 + k_y^2 + k_z^2}.$$

The new dispersion relation depends on the spatial sampling rates

$$n_\alpha = \frac{2\pi}{|k_\alpha|\Delta\alpha}, \quad (\alpha = x, y, z), \tag{25}$$

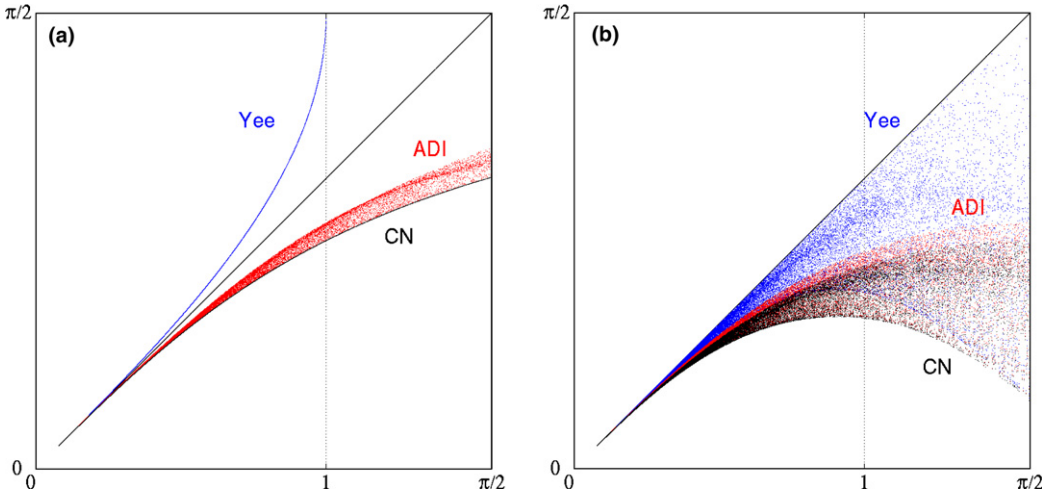

Fig. 1. Dispersion relations θ vs. θ exact for the CN, ADI and Yee schemes for (a) $\Delta\alpha \to 0$ ($f(\phi) = 1$) and (b) finite $\Delta\alpha$ ($f(\phi)$ as in (6)). A set of 360^2 triplets $(k_x, k_y, k_z) = k(\cos\varphi\cos\psi, \cos\varphi\sin\psi, \sin\varphi)$ uniformly distributed in the square $[\varphi, \psi] = [0, \pi/2]^2$ and 360^2 sampling rates $(n_x = n_y = n_z, m) = m(1/\sqrt{3}, 1)$ with m uniformly distributed in the interval [2] was used.

the time sampling rate $m = \frac{2\pi}{\omega\Delta t}$ ($\omega = k$ in scaled variables, compared to the usual relation $\omega = kc$ in unscaled variables), as well as on the particular spatial discretization used (i.e., f as in (6)). The range $0 \leqslant \theta_{\text{exact}} \leqslant \frac{\pi}{2}$ corresponds to the Nyquist limit $n_\alpha \geqslant 2$. Fig. 1, right, illustrates the dispersion relation for a range $2 \leqslant m_x = m_y = m_z = m \leqslant 40$ of random spatial samplings for a staggered grid with f given by (6), in the case $n = m\sqrt{3}$ associated to the CFL stability limit of the Yee scheme [21]. The dispersion relation for the Yee scheme is included for comparison. For the semi-discretized problem (in time) the Yee curve is above the diagonal line $\theta = \theta_{\text{exact}}$ (typical of an explicit, conditionally stable, scheme), while the CN and ADI "curves" are below (typical of implicit, unconditionally stable schemes). Because of (7) spatial discretization lowers these curves. In particular, exact dispersion properties can be recovered in the Yee case for a special choice of Δt [16]. Although this cannot be done in the CN or ADI cases, upper bounds on Δt can be obtained to reach a specific dispersion accuracy (e.g. see [14,15,24] in the ADI case).

3.2. Accuracy (small W)

The accuracy of the different numerical schemes is evaluated by determining the leading ($\mathcal{O}(\Delta t^3)$) truncation error in the approximation of the exact semigroup $e^{2(A+B)}$ by the iteration matrix of the schemes. We obtain

$$e^{2(A+B)} - T_{\text{CN}} = -\frac{2}{3}(A+B)^3 + \mathcal{O}(W^4) \tag{26}$$

and

$$e^{2(A+B)} - T_{\text{ADI}} = -\frac{2}{3}(A+B)^3 + 2AB(A+B) + \mathcal{O}(W^4) \tag{27}$$

for the CN and ADI schemes (compare Eq. (22) in [8]). The extra term in (27) compared to (26) is often blamed for the lower accuracy observed in certain ADI experiments with highly refined grids (i.e., $n_\alpha \gg \text{CFL}$), as in the experiments conducted in [19]. With (6) the relations (8b), (7), (10), (25) then yield

$$|W_\alpha| = \frac{1}{2}\Delta t|\tilde{k}_\alpha| \leqslant \frac{1}{2}\Delta t|k_\alpha| \leqslant \frac{1}{2}\Delta\alpha|k_\alpha|\text{CFL} = \pi\frac{\text{CFL}}{n_\alpha} \ll 1, \tag{28}$$

which justifies the expansions (26) and (27). A detailed computation for a two-dimensional TE_z wave yields (with A and B given by (B.1), $W_z = 0$)

$$E_{\mathrm{CN}} \equiv -\frac{2}{3}(A+B)^3 = \frac{2}{3}\mathrm{j}\begin{bmatrix} 0 & 0 & -W_y W^2 \\ 0 & 0 & W_x W^2 \\ -W_y W^2 & W_x W^2 & 0 \end{bmatrix}$$

while

$$E_{\mathrm{ADI}} \equiv -\frac{2}{3}(A+B)^3 + 2AB(A+B) = \frac{2}{3}\mathrm{j}\begin{bmatrix} 0 & 0 & 3W_x^2 W_y - W_y W^2 \\ 0 & 0 & W_x W^2 \\ -W_y W^2 & W_x W^2 & 0 \end{bmatrix}.$$

The Euclidean norms of E_{CN} and E_{ADI} satisfy $\|E_{\mathrm{CN}}\| = \frac{2}{3}W^3 \leqslant \|E_{\mathrm{ADI}}\|$ for all wave directions, with a strict inequality whenever $|W_x| \geqslant |W_y|\sqrt{2}$.

4. Iterated ADI schemes

In an effort to reduce anisotropy effects in dispersion properties and accuracy degradation in large gradient locations in ADI calculations, Wang et al. recently considered the iteration

$$(I-A)(I-B)u_{k+1}^{n+1} = (I+A)(I+B)u^n + AB(u_k^{n+1} - u^n) \tag{29}$$

for solving (12) [19]. If $u_0^{n+1} = u^n$ the first iterate u_1^{n+1} is simply the approximation obtained with the ADI scheme (13).

Numerical tests conducted in [8] on a 2D TE_z wave suggest that more accuracy can be gained, in particular around grid locations close to field singularities or sharp gradients, by using a small number of iterations (29). However, no theoretical justification is given. In this section we show that the fixed point iteration (29) indeed converges as k increases (to the CN approximation) and investigate the stability/accuracy properties of the iterated schemes resulting from a fixed number k of fixed-point iterations.

4.1. Split forms

Wang et al. use the split form

$$(I-A)u_{k+1}^{n+\frac{1}{2}} = (I+B)u^n + \frac{1}{2}AB(u_k^{n+1} - u^n), \tag{30a}$$

$$(I-B)u_{k+1}^{n+1} = (I+A)u_{k+1}^{n+\frac{1}{2}} + \frac{1}{2}AB(u_k^{n+1} - u^n) \tag{30b}$$

of (29), which enables them the same efficiency as ADI [19]. They also suggest replacing u_k^{n+1} in (30b) by a linear prediction but provide no specific detail.

The form (30) offers no specific advantage over the simpler split form

$$(I-A)u_{k+1}^{*} = (I+A)(I+B)u^n + AB(u_k^{n+1} - u^n),$$
$$(I-B)u_{k+1}^{n+1} = u_{k+1}^{*},$$

other than the interpretation of $u_{k+1}^{n+\frac{1}{2}}$ as an approximate solution at the intermediate time $(n+\frac{1}{2})\Delta t$. On the other hand, the alternate split form

$$(I-A)u_{k+1}^{n+\frac{1}{2}} = u^n + B\frac{u_k^{n+1} + u^n}{2}, \tag{31a}$$

$$(I-B)\frac{u_{k+1}^{n+1} + u^n}{2} = u^n + Au_{k+1}^{n+\frac{1}{2}}, \tag{31b}$$

of (29) involves only multiplications by A or B (first-order derivatives) rather than AB (second-order derivatives) and can be expected to be less prone to round-off errors in the numerical differentiation process. As in the ADI case $u_{k+1}^{n+\frac{1}{2}}$ and u_{k+1}^{n+1} can be efficiently computed via tridiagonal solves whose right-hand sides require second-order differentiation, rather than third-order if (30) is used, see Appendix C. Note that $u_{k+1}^{n+\frac{1}{2}}$ defined in (30a) and (31a) are distinct, although both are consistent approximations of u at $(n+\frac{1}{2})\Delta t$.

4.2. Convergence of the fixed-point iteration (29)

The fixed point iteration (29) converges if the eigenvalues μ of the iteration matrix

$$S_{\mathrm{FP}} = (I-B)^{-1}(I-A)^{-1}AB = (I-B)^{-1}\Big[(I-A)^{-1}AB(I-B)^{-1}\Big](I-B)$$
$$= (I-B)^{-1}\Big[(I-A)^{-1}A(I-B)^{-1}\Big](I-B) = (I-B)^{-1}\mathscr{C}(A)\mathscr{C}(B)(I-B), \tag{32}$$

where

$$\mathscr{C}(A) = (I-A)^{-1}A,$$

satisfy $|\mu| < 1$. Fig. 2 (left) numerically confirms that this is indeed true independently of the wave number (k_x, k_y, k_z). Note that the version of the fixed-point iteration based on linear prediction does not converge.

We now justify why the fixed point iteration (29) does converge. Since S_{FP} is similar to $\mathscr{C}(A)\mathscr{C}(B)$ it suffices to show that this is true for the eigenvalues μ of $\mathscr{C}(A)\mathscr{C}(B)$. The matrix A is skew-Hermitian, so that its eigenvalues jw are located on the imaginary axis. The eigenvalues $\mathscr{C}(\mathrm{j}w)$ of $\mathscr{C}(A)$ then satisfy

$$|\mathscr{C}(\mathrm{j}\omega)| = \left|\frac{\mathrm{j}\omega}{1-\mathrm{j}\omega}\right| = \frac{|\omega|}{\sqrt{1+\omega^2}} < 1.$$

A similar bound holds for the skew-Hermitian matrix B. However, this is not sufficient to prove the result, since the eigenvalues of AB cannot be simply obtained from those of A and B because A and B do not commute. Instead, we show that the Euclidean norms $\|\mathscr{C}(A)\|$, $\|\mathscr{C}(B)\| < 1$. The matrix

$$\mathscr{C}(A)\mathscr{C}(A)^* = (I-A)^{-1}AA^*[(I-A)^{-1}]^* = (I-A)^{-1}AA^*(I-A^*)^{-1} = -(I-A)^{-1}A^2(I+A)^{-1}$$
$$= -(I-A^2)^{-1}A^2 = -\mathscr{C}(A^2)$$

has eigenvalues

$$0 \leqslant -\mathscr{C}((\mathrm{j}\omega)^2) = \frac{\omega^2}{1+\omega^2} < 1,$$

so that

$$\|\mathscr{C}(A)\|^2 = \max_{\lambda}\lambda(\mathscr{C}(A)\mathscr{C}(A)^*) = \max_{\omega}\frac{\omega^2}{1+\omega^2} < 1. \tag{33}$$

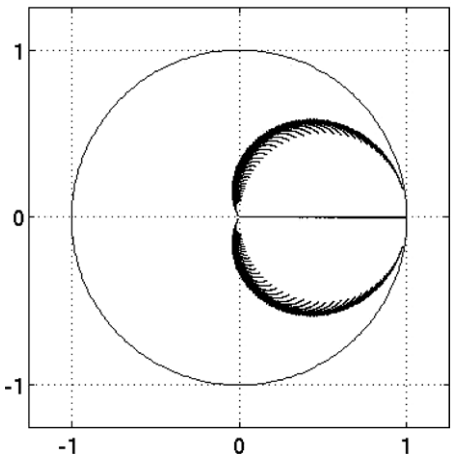

Fig. 2. Eigenvalues of the iteration matrix S_{FP} (32) of the fixed-point iteration (29) for 50^3 triplets (W_x, W_y, W_z) logarithmically distributed in the cube $[10^{-1}, 10^1]^3$.

Similarly, $\|C(B)\| < 1$. Consequently,

$$|\mu| \leqslant \|\mathscr{C}(A)\mathscr{C}(B)\| \leqslant \|\mathscr{C}(A)\| \, \|\mathscr{C}(B)\| \leqslant 1.$$

The bound (33) suggests a fast convergence of the FP iteration for small ω i.e., small W, which occurs in highly refined grids and relatively large CFL numbers (see (28)).

4.3. Stability/dispersion

4.3.1. 2D wave

We first consider a 2D TE_z/TM_z wave ($k_z = 0, W_z = 0$). Remarkably, $T_{ADI(k)}$ possesses eigenvalues of the form (16) (three associated to a TE_z mode, and the same three associated to a TM_z mode) for any k, with an angle $\theta = \theta_{ADI(k)}$ which can be expressed via the dispersion relation

$$\cos\theta_{ADI(k)} = \cos\theta_{CN}\sqrt{1-\rho^k} \tag{34}$$

with ρ given by (20) ($Q_{ADI(I)} = \theta_{ADI}$), see Appendix B for a detailed proof. In particular

$$\theta_{CN} \leqslant \cdots \leqslant \theta_{ADI(2)} \leqslant \theta_{ADI} \leqslant \theta_{exact}$$

(with equality in all but the last inequality if $W_x = 0$ or $W_y = 0$). Fig. 3 displays the relative phase accuracy $\theta_{ADI(k)}/\theta_{exact}$ in terms of the wave direction. The dispersion accuracy of the ADI(k) scheme monotonically decreases with k but becomes more isotropic. The convergence is faster at higher spatial sampling rates/CFL ratios.

In the 2D case the fixed-point iteration (29) thus defines unconditionally stable schemes whose dispersion properties monotonically approach those of the CN scheme.

4.3.2. 3D wave

For the general case of a 3D wave, the spectral radius of the iteration matrices $T_{ADI(k)}$ is determined numerically for a range of random wave numbers. The result is plotted against W in Fig. 4 ($W \simeq$ CFL for poorly resolved wave numbers, see (28)). Although both ADI (the starting scheme) and CN (the limiting scheme) are unconditionally stable, all intermediate iterated schemes appear to be conditionally stable only. First the ADI(2) scheme exhibits worse stability properties than the Yee scheme itself (unstable for values $W < 1$). As k increases the stability limit seems to slowly increase too. Note however how a number of modes develop instabilities at lower values of W as k further increases. It turns out such a layer of unstable modes also exists at smaller values of k, but is so thin that it is not apparent in Fig. 4. As a result all practical iterated schemes ($k < 10$) are unstable at CFL ≈ 2, and lead to a blow-up in the numerical solution.

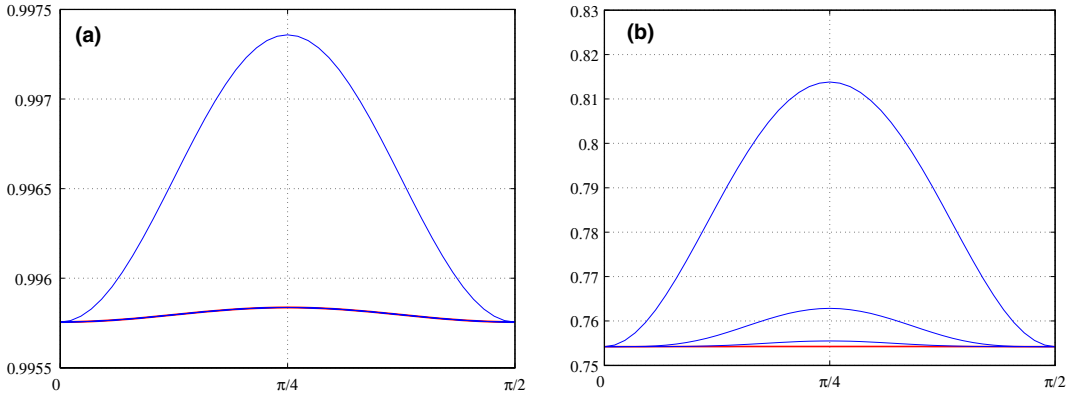

Fig. 3. Relative phase velocity $\theta_{ADI(k)}/\theta_{exact}$ with increasing k for a 2D wave $(k_x, k_y) = k(\cos(\varphi), \sin(\varphi))$ vs. φ in the case of a highly refined uniform spatial grid ($n_x = n_y = 100$ cells per wavelength) and (a) CFL = 5, (b) CFL = 50 ($\Delta z = \infty$).

The time it takes to observe a macroscopic effect of the blow-up can be estimated for a constant Δt as follows. If $\rho = 1 + \varepsilon$ denotes the spectral radius of the iteration matrix $T_{\mathrm{ADI}(k)}$, and the numerical solution is of order $\mathcal{O}(1)$ before blow-up, then the instability becomes visible after a time $t_{\text{blow-up}} = n\Delta t$ such that $(1+\varepsilon)^n = \mathcal{O}(1)$. This requires $\varepsilon \approx \frac{C}{n}$ for some constant C (because $\lim_{n\to\infty}(1+\frac{C}{n})^n = e^C = \mathcal{O}(1)$), i.e.,

$$t_{\text{blow-up}} \approx \frac{C\Delta t}{\varepsilon}. \tag{35}$$

Table 1 lists the blow-up time estimates vs. $1 < k \leqslant 10$ at CFL $= 2$ with $\Delta t \approx 0.058$ and choosing $C = 20$. The actual blow-up time obtained from the numerical simulations in Section 5 is included for comparison.

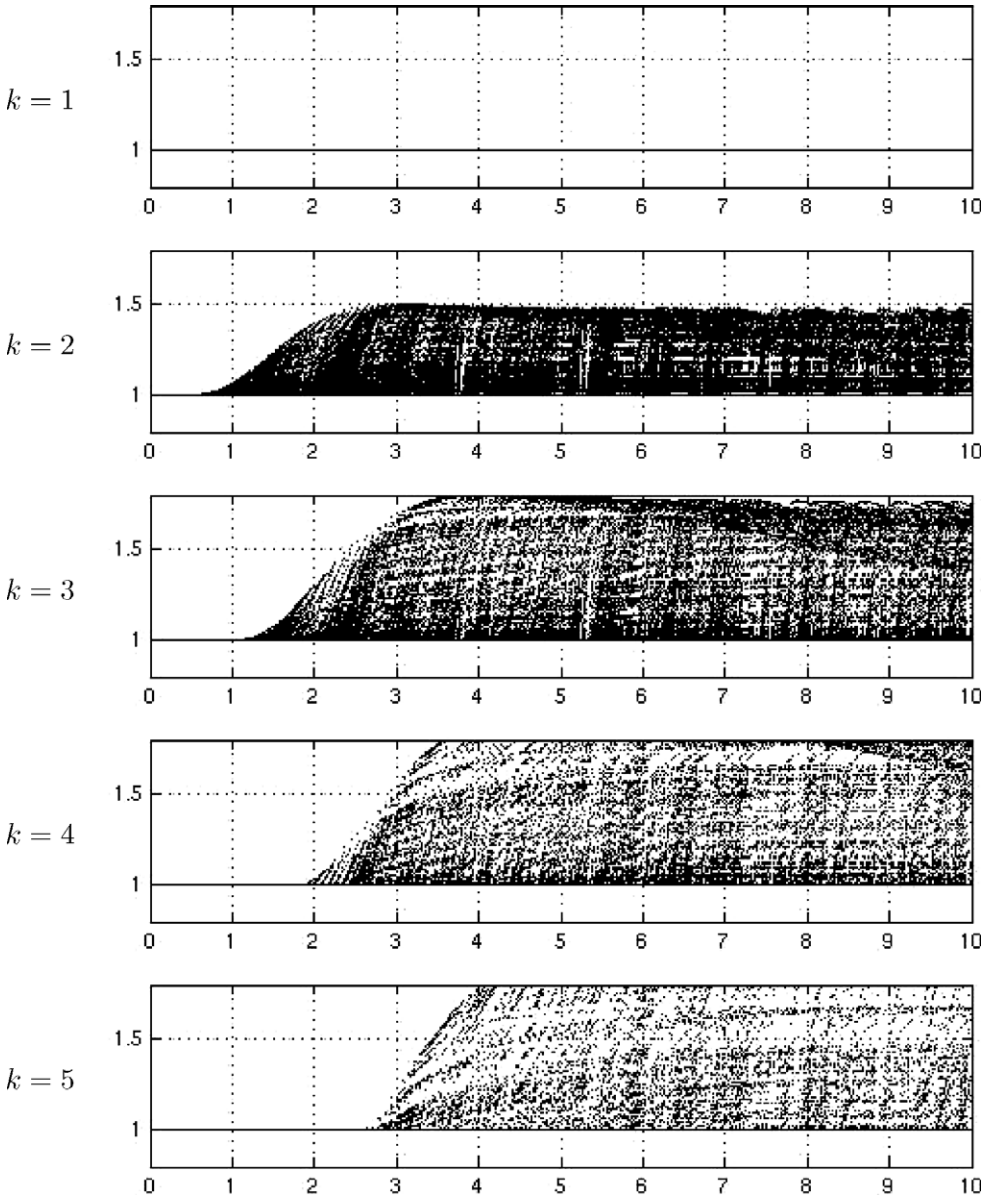

Fig. 4. Spectral radius of the iteration matrix $T_{\mathrm{ADI}(k)}$ from (36) of iterated schemes for $k = 1,\ldots,10$ as a function of W using 50^3 random triplets (W_x, W_y, W_z) logarithmically distributed in the cube $[10^{-1}, 10^{1}]^3$.

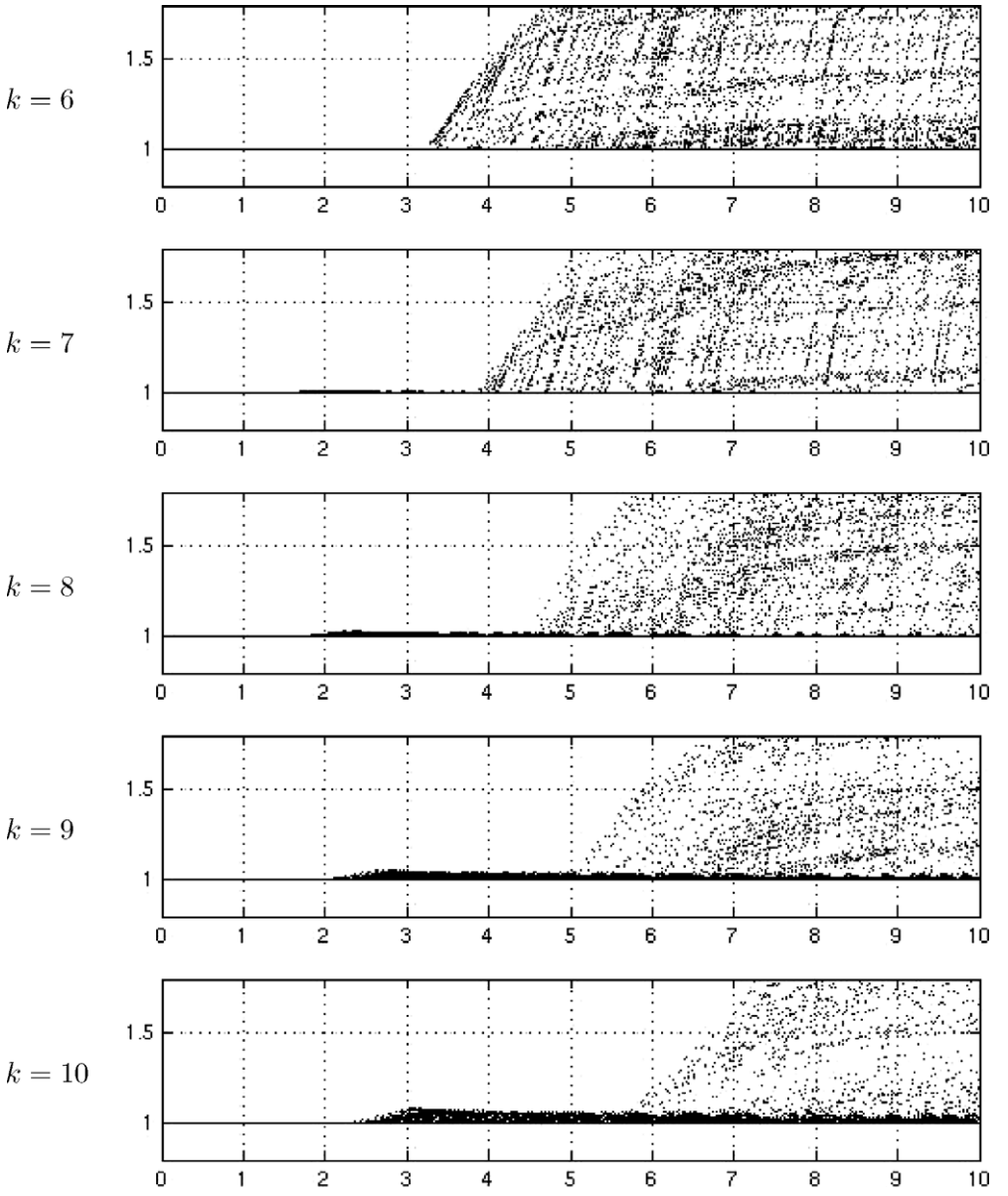

Fig. 4 (*continued*)

Because the spectral radius of $T_{\mathrm{ADI}(k)}$ is sampled on a finite number of random wave numbers, the estimated values of $t_{\text{blow-up}}$ only yield an upper bound on the actual values. They also become increasingly inaccurate as ε gets smaller, but still provide a reasonable guideline to observe the instability at the macroscopic level.

4.4. Accuracy

The iteration matrix of the scheme obtained after k fixed point iterations (29) is obtained recursively from

$$T_{\mathrm{ADI}(k+1)} = T_{\mathrm{ADI}} + (I - B)^{-1}(I - A)^{-1}AB(T_{\mathrm{ADI}k} - I) \tag{36}$$

with $T_{\mathrm{ADI}(k+1)} = I(T_{\mathrm{ADI}(1)} = T_{\mathrm{ADI}})$.

Table 1
Maximal spectral radius of $T_{ADI(k)}$ over 50^2 random triplets (W_x, W_y, W_z) with $W_x^2 + W_y^2 + W_z^2 = 4$ logarithmically distributed in the square $[10^{-1}, 10^{1}]^2$ ($W = 2 \simeq$ CFL), estimated and actual time to blow-up (using (35) with $C \simeq 20$ and simulations from Section 5)

k	Max spectral radius $1 + \varepsilon$	Estimated ($t_{\text{blow-up}}$)	Actual ($t_{\text{blow-up}}$)
1	1.000000	∞	∞
2	1.399842	3	3
3	1.305731	4	4
4	1.037640	31	27
5	1.000063	18,358	2080
6	1.002654	435	171
7	1.013163	88	54
8	1.018689	62	61
9	1.003921	294	327
10	1.000013	84,051	14,200

The first iteration of the iterated ADI scheme (36) yields

$$e^{2(A+B)} - T_{ADI(2)} = e^{2(A+B)} - T_{ADI} - (I-B)^{-1}(I-A)^{-1}AB(T_{ADI} - I)$$
$$= -\frac{2}{3}(A+B)^3 + 2AB(A+B) - AB(2(A+B)) + {}_0(W^3) = -\frac{2}{3}(A+B)^3 + {}_0(W^3), \qquad (37)$$

i.e., a leading error term similar to that of the CN scheme. Subsequent iterations do not modify this leading term.

5. Numerical experiments

We illustrate the behavior of the ADI(k) schemes when applied to a unit box $[0,1]^3$ with PEC boundary conditions. The spatial discretization used corresponds to the classical centered and staggered scheme of Yee ([21], see Fig. 5) with mesh size $\Delta x = \Delta y = \Delta z = \frac{1}{20}$. The boundary condition for the E_z component at $y = 0$ is a plane wave

$$E_z = \sin 2\pi(t + x + \sigma z) \qquad (38)$$

with frequency 1. All other electric boundary as well as initial conditions are set to zero. The iterated schemes are implemented using the update equations listed in Appendix C. The E_z electric field component is then observed at the center of the box.

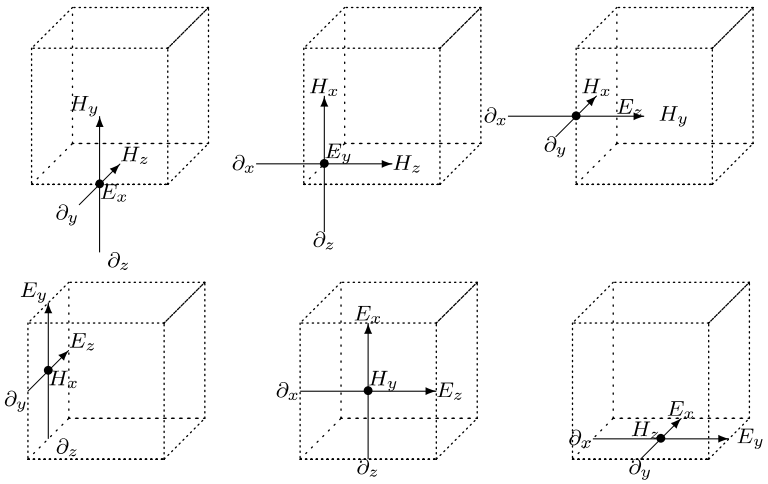

Fig. 5. Staggered grid finite differentiation as in the Yee scheme [21]. Electric field values E_x, E_y, E_z are defined at the middle of edges in the x, y, z directions, respectively, while magnetic field values H_x, H_y, H_z are defined at the center of faces in the planes orthogonal to the x, y, z directions, respectively.

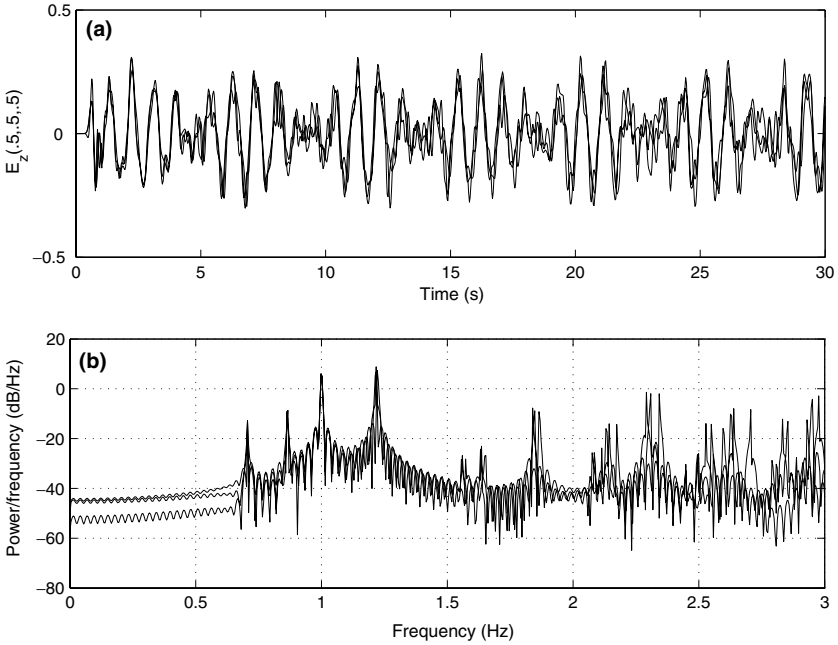

Fig. 6. (a) Time series for $E_z(.5,.5,.5)$ obtained with the Yee, ADI(1)=ADI and ADI(5) schemes at CFL $= 1$ with $\sigma = 1$ in the boundary condition (38). (b) Corresponding power spectrum density (based on time series for $0 \leqslant t \leqslant 200$). The ADI(5) spectrum is closer to the Yee spectrum than the ADI(l) is for larger frequencies.

The (Matlab) code for ADI(k) is validated against the Yee solution at CFL $= 1$ for $k = 1$ (ADI) and $k = 5$ by plotting the time series of $E_z(.5,.5,.5)$ as well as the corresponding power spectrum densities obtained in the time interval $0 \leqslant t \leqslant 200$, see Fig. 6. Note the dominant mode at 1 Hz, as well as the presence of harmonics. The lower modes match perfectly.

5.1. 3D experiments: $\sigma = 1$

Nonzero values of σ in the boundary condition (38) introduce a z-dependence and a coupling between TE and TM modes. Because a variety of modes coupling TE and TM components are excited, the schemes ADI(k), $k > 1$, are expected to be unstable according to the stability analysis of Section 4, see Fig. 4.

Fig. 7 displays the time series at CFL $= 2$ for increasing values of k. The ADI(2), ADI(3) and ADI(4) solutions rapidly become unstable, in a time frame consistent with the estimates of Table 1. The ADI(1) = ADI solution remains stable, as expected.

Running the ADI(5) scheme a while longer reveals instabilities which become apparent around $t_{\text{blow-up}} = 2080$ s, while instabilities in ADI(k), $k = 6,7,8,9$, develop in a much shorter time frame. These results are in agreement with the behavior expected from the numerical stability analysis conducted in Section 4 on single Fourier modes.

5.2. 2D experiments: $\sigma = 0$

Setting $\sigma = 0$ in the boundary condition (38) results into a decoupling of TE and TM modes similar to the one occurring in a two-dimensional implementation of the problem. Fig. 8 displays, as in Fig. 7, the time series of $E_z(.5,.5,.5)$ for the schemes ADI(k), $k = 1,2,3$. The iterations ADI(2) and ADI(3) are now stable, which supports the conclusions of Section 4.3. Moreover, a difference can be observed between the time series for ADI and ADI(2). On the other hand no noticeable difference between the time series for ADI(2) and ADI(3) exist, in agreement with the accuracy estimate of Section 4.4. Tests with larger values of k show no change in the time series.

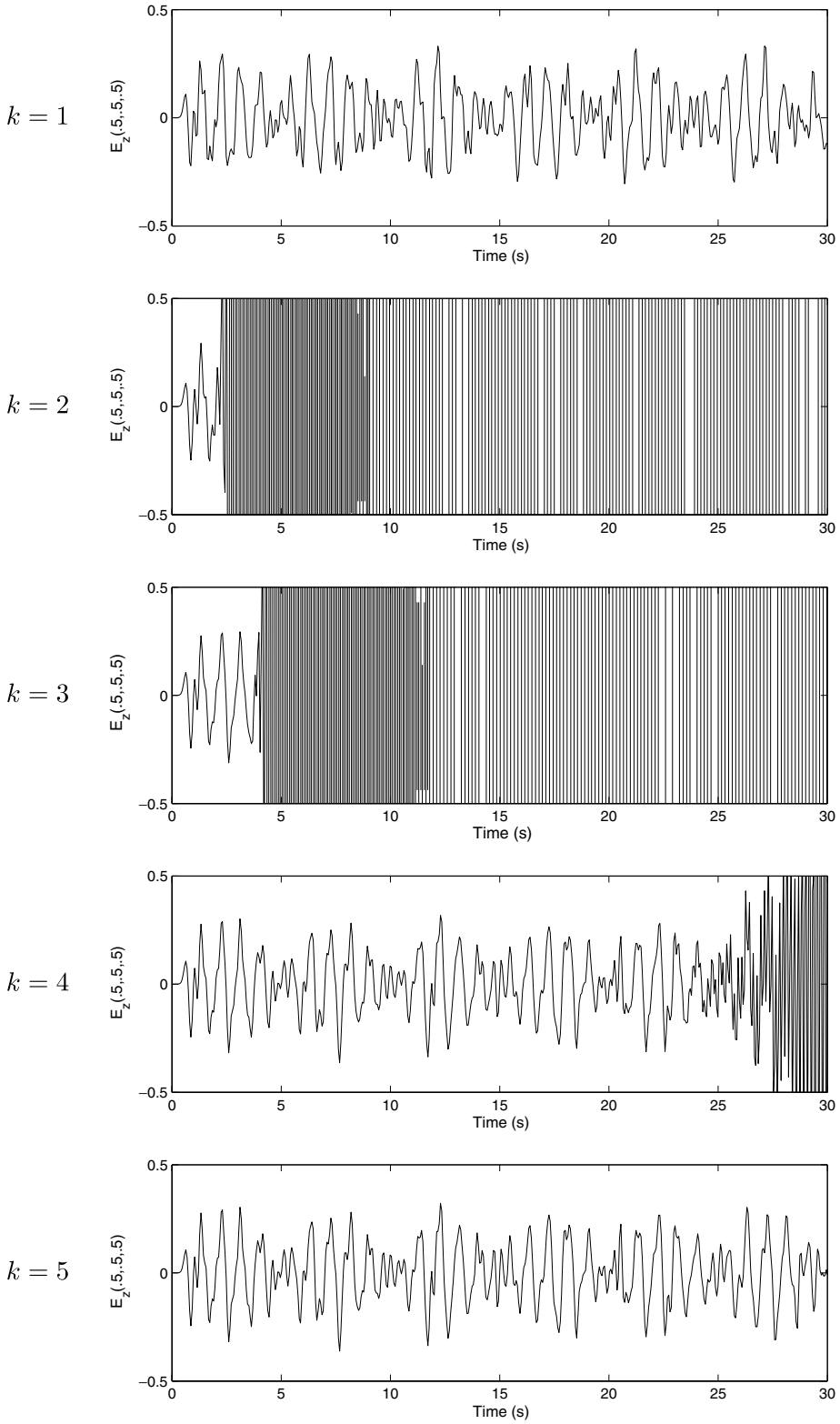

Fig. 7. Time series for $E_x(.5,.5,.5)$ obtained with ADI(k) for $k = 1,2,3,4,5$, using $\sigma = 1$ in (38) (CFL = 2). In (e) the series blows up at time $t \approx 2080$, see Table 1.

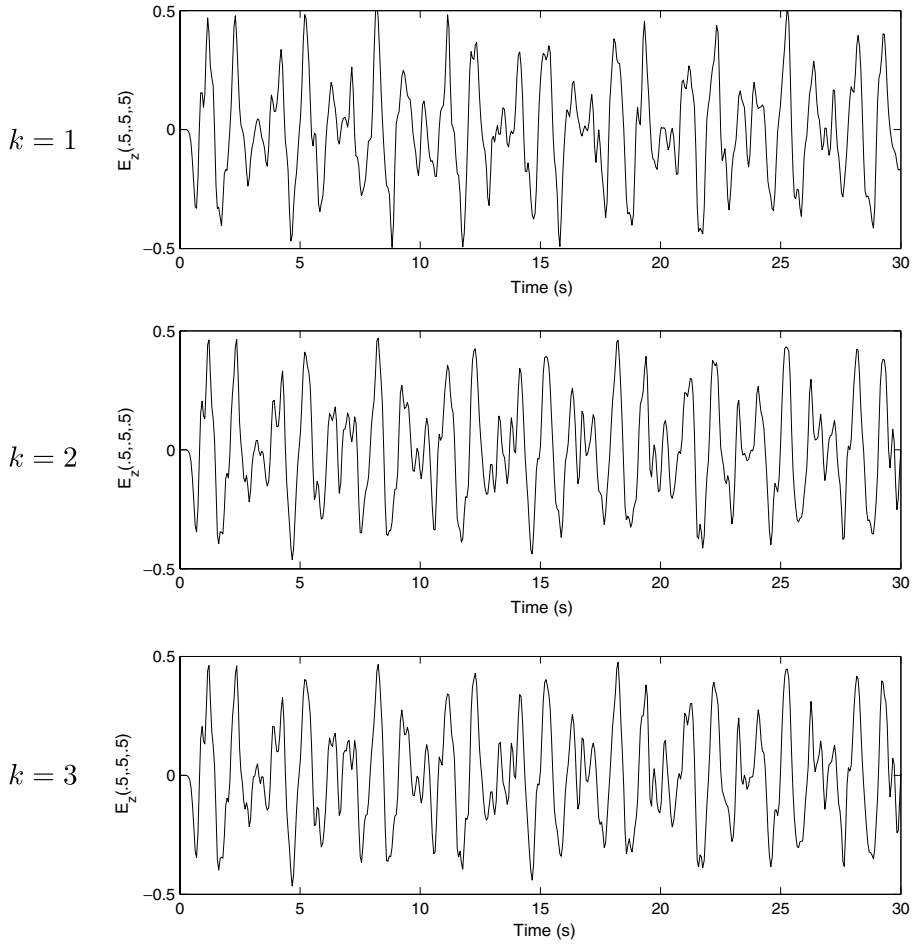

Fig. 8. Time series for $E_x(.5,.5,.5)$ obtained with ADI(k) for $k = 1,2,3$, using $\sigma = 0$ in (38) (CFL $= 2$). In this 2D simulation, no blow-up occurs, compare with a 3D simulation, Fig. 7.

6. Conclusions

The iterated ADI(2) scheme obtained with a single step of fixed-point iteration appears to be a good substitute for the CN scheme in 2D simulations: both schemes possess similar unconditional stability and accuracy properties when applied to non-dissipative Maxwell curl system (TE or TM modes). However, the coupling of TE and TM modes in three dimensions destabilizes the iterated schemes ADI(k) for $k > 1$. These schemes exhibit only marginal improvements in stability properties (and in a non monotonic fashion as k increases) and at a cost which rapidly becomes prohibitive. Unresolved (high frequency) modes in the solution are typically responsible for igniting the instabilities.

Overall, there seems to be little incentive in using the ADI(k) schemes analyzed in this work as a substitute for the CN scheme in problems with coupled TE/TM modes, the usual case in full 3D simulations. If one is interested in low band analysis of a solution (e.g. in low frequency bioelectromagnetics) using a highly refined grid (a situation where ADI is more efficient than the Yee scheme), it might be possible to recover useful power spectral information before blow-up occurs, as in Fig. 6. A low passband filtering of the numerical solution at each time step might improve the stability properties of the ADI(k) scheme in long term calculations.

The difference in stability properties between the 2D and 3D cases does not seem to be specific to the iterated schemes discussed here. A similar scenario applies to a symmetric version of ADI proposed in [20] as well as schemes with corrections based on linear extrapolation proposed in [1]. The construction of an ADI-like scheme with better accuracy/dispersion properties (which deal with the low W range) than the standard

ADI scheme, and unconditional stability (which addresses the behavior of the method for large W) when applied to problems with coupled TE/TM modes is currently under way.

Acknowledgements

The author thanks the three anonymous reviewers for their careful reviewing of the manuscript and their constructive remarks.

Appendix A. Unconditional stability of ADI

A.1. Via a polar decomposition [3]

Write

$$T_{\mathrm{ADI}} = (I-B)^{-1}C_A C_B (I-B),$$

where

$$C_A = (I-A)^{-1}(I+A), \quad C_B = (I-B)^{-1}(I+B)$$

are the Cayley transforms of A and B, respectively. Since A and B are skew-Hermitian, the matrices C_A and C_B are unitary. Using $\|(I-B)^{-1}\| \leqslant 1$ we obtain

$$\|T^n_{\mathrm{ADI}}\| = \|(I-B)^{-1}(C_A C_B)^n (I-B)\| \leqslant \|(I-B)^{-1}\|\|I-B\| \leqslant \sqrt{1+\max(W_x^2, W_y^2, W_z^2)}$$

independently of n (but not independently of the wave number).

A.2. Via an energy estimate [4,5]

Since A and B are skew-hermitian w.r.t. the Euclidean inner product $(u,v) = v^* u$ we have $\Re(u,Au) = \Re(u,Bu) = 0$ for all u. The energy functional

$$\mathscr{E}(u) = \|u\|^2 + \|Bu\|^2 \tag{A.1}$$

then satisfies

$$\begin{aligned}\mathscr{E}(u^{n+1}) &= \|u^{n+1}\|^2 + \|Bu^{n+1}\|^2 = \|u^{n+1} - Bu^{n+1}\|^2 + 2\Re(u^{n+1}, Bu^{n+1}) = \|(I-B)u^{n+1}\|^2 = \|(I+A)u^{n+\frac{1}{2}}\|^2 \\ &= \|u^{n+\frac{1}{2}} - Au^{n+\frac{1}{2}}\|^2 + 4\Re(u^{n+\frac{1}{2}}, Au^{n+\frac{1}{2}}) = \|(I-A)u^{n+\frac{1}{2}}\|^2 = \|(I+B)u^n\|^2 \\ &= \|u^n\|^2 + \|Bu^n\|^2 + 2\Re(u^n, Bu^n) = \|u^n\|^2 + \|Bu^n\|^2 = \mathscr{E}(u^n).\end{aligned}$$

Note that the energy (A.1) depends on B i.e., the wave number. Higher wave numbers yield a larger, but constant, energy level.

A.3. Comments

The skew-Hermitian property of A and B plays a fundamental role in the above stability proofs. This property holds for the staggered grid second-order finite difference scheme of Yee [21], and selected higher-order spatial difference schemes [17,2]. The energy estimate of Appendix A.2 also extends directly to lossy media, where $\Re(u,Au), \Re(u,Bu) \leqslant 0$.

Appendix B. Proof of (16) and (34) for $T_{\mathrm{ADI}(k)}$

When $k_z = 0 (W_z = 0)$ the matrices A and B can be simultaneously partitioned into two 3×3 block matrices corresponding to one TE_z wave propagation problem and one TM_z wave propagation problem. For simplicity, we only consider here the TE_z case and rewrite

$$A = \begin{bmatrix} 0 & 0 & -\mathrm{j}W_y \\ 0 & 0 & 0 \\ -\mathrm{j}W_y & 0 & 0 \end{bmatrix}, \quad B = \begin{bmatrix} 0 & 0 & 0 \\ 0 & 0 & \mathrm{j}W_x \\ 0 & \mathrm{j}W_x & 0 \end{bmatrix}. \tag{B.1}$$

W.l.o.g. we assume $W_x W_y \neq 0$ (if $W_x W_y = 0$ then $AB = 0$ and $T_{\mathrm{ADI}(k)} = T_{\mathrm{CN}}$ for all $k > 0$). We obtain

$$S_{\mathrm{FP}} = (I - B)^{-1}(I - A)^{-1}AB = \rho P$$

with ρ given by (20) and

$$P = \begin{bmatrix} 0 & (1 + W_x^2)/W_x S W_y & 0 \\ 0 & 1 & 0 \\ 0 & -\mathrm{j}/W_x & 0 \end{bmatrix}.$$

Note that $0 < \rho < 1$ and $P^2 = P$ (projection matrix). In particular $I - \rho P$ is nonsingular. By induction the iteration matrix $T_{\mathrm{ADI}(k)}$ obtained from (36) satisfies

$$\begin{aligned} T_{\mathrm{ADI}(k)} - I &= T_{\mathrm{ADI}} - I + \rho P(T_{\mathrm{ADI}(k-1)} - I) = T_{\mathrm{ADI}} - I + \rho P(T_{\mathrm{ADI}} - I + \rho P(T_{\mathrm{ADI}(k-2)} - I)) = \cdots \\ &= (I + \rho P + \cdots + (\rho P)^{k-1})(T_{\mathrm{ADI}} - I) = (I - \rho^k P)(I - \rho P)^{-1}(T_{\mathrm{ADI}} - I). \end{aligned}$$

Letting $k \to \infty$ yields

$$T_{\mathrm{CN}} - I = (I - \rho P)^{-1}(T_{\mathrm{ADI}} - I)$$

so that

$$T_{\mathrm{ADI}(k)} - I = (I - \rho^k P)(T_{\mathrm{CN}} - I).$$

Using the spectral decomposition $A + B = Q\Lambda Q^{\mathrm{T}}$ with

$$\Lambda = \begin{bmatrix} 0 & & \\ & \mathrm{j}W & \\ & & -\mathrm{j}W \end{bmatrix}, \quad Q = \frac{1}{w\sqrt{2}} \begin{bmatrix} W_x\sqrt{2} & -W_y & W_y \\ W_y\sqrt{2} & W_x & -W_x \\ 0 & W & W \end{bmatrix},$$

where $W = \sqrt{W_x^2 + W_y^2}$ (note $Q^{\mathrm{T}}Q = I$) we obtain

$$T_{\mathrm{CN}} = Q\Lambda_{\mathrm{CN}}Q^{\mathrm{T}}, \quad \Lambda_{\mathrm{CN}} = \begin{bmatrix} 1 & & \\ & \xi & \\ & & \bar{\xi} \end{bmatrix}, \quad \xi = \frac{1 + \mathrm{j}W}{1 - \mathrm{j}W}.$$

Consequently,

$$\begin{aligned} Q^{\mathrm{T}}T_{\mathrm{ADI}(k)}Q &= Q^{\mathrm{T}}T_{\mathrm{CN}}Q - \rho^k Q^{\mathrm{T}}P(T_{\mathrm{CN}} - I)Q = \Lambda_{\mathrm{CN}} - \rho^k Q^{\mathrm{T}}PQ(\Lambda_{\mathrm{CN}} - I) \\ &= \begin{bmatrix} 1 & & \\ & \xi & \\ & \bar{\xi} & \end{bmatrix} - \frac{\rho^k}{2W^2} \begin{bmatrix} \star & \star & \star \\ \star & -\mu & \mu \\ \star & \bar{\mu} & -\bar{\mu} \end{bmatrix} \begin{bmatrix} 0 & & \\ & \xi - 1 & \bar{\xi} - 1 \end{bmatrix} = \begin{bmatrix} 1 & \star & \star \\ 0 & \xi(1 + \mathrm{j}\frac{\rho^k}{w}) & \mathrm{j}\frac{\rho^k}{w} \\ 0 & -\mathrm{j}\frac{\rho^k}{w} & \bar{\xi}(1 - \mathrm{j}\frac{\rho^k}{w}) \end{bmatrix} \end{aligned}$$

with $\mu = 1 + \mathrm{j}W$ (stars indicate coefficients which are not of interest). The eigenvalues of $T_{\mathrm{ADI}(k)}$ thus are $\lambda = 1$ and the roots of the characteristic equation

$$\lambda^2 - 2\Re\left(\xi\left(1 + \mathrm{j}\frac{\rho^k}{w}\right)\right)\lambda + 1 = 0.$$

Since

$$-1 < \Re\left(\xi\left(1 + \mathrm{j}\frac{\rho^k}{w}\right)\right) = 1 - \frac{2(\rho^k + W^2)}{1 + W^2} < 1$$

the two roots of the quadratic equation are complex conjugate, and have modulus one (their product is 1). This shows that the eigenvalues of $T_{\mathrm{ADI}(k)}$ are of the form (16) with

$$\cos^2\theta_{\mathrm{ADI}(k)} = \frac{1}{2}\left(1+\cos(2\theta_{\mathrm{ADI}(k)})\right) = \frac{1}{2}\left(1+\Re\left(\xi\left(1+\mathrm{j}\frac{\rho^k}{k}\right)\right)\right) = \frac{1-\rho^k}{1+W^2} = (1-\rho^k)\cos^2\theta_{\mathrm{CN}}.$$

Appendix C. Practical implementation of (31)

In the following $(\alpha,\beta,\gamma) = (x,y,z)$, $(y,\ z,x)$, (z,x,y).

C.1. Update equations for (31a)

$$\left(I-\left(\frac{\Delta t}{2}\right)^2\partial_{\beta,\beta}\right)E^{n+\frac{1}{2}}_{\alpha,k+1} = E^n_\alpha + \frac{\Delta t}{2}\partial_\beta H^n_\gamma - \frac{\Delta t}{2}\partial_\gamma\frac{H^n_\beta + H^{n+1}_{\beta,k}}{2} - \left(\frac{\Delta t}{2}\right)^2\partial_{\alpha,\beta}\frac{E^n_\beta + E^{n+1}_{\beta,k}}{2},$$

$$H^{n+\frac{1}{2}}_{\gamma,k+1} = H^n_\gamma + \frac{\Delta t}{2}\partial_\beta E^{n+\frac{1}{2}}_{\alpha,k+1} - \frac{\Delta}{2}\partial_\alpha\frac{E^n_\beta + E^{n+1}_{\beta,k}}{2}.$$

C.2. Update equations for (31b)

$$\left(I-\left(\frac{\Delta t}{2}\right)^2\partial_{\gamma,\gamma}\right)\frac{E^{n+1}_{\alpha,k+1}}{2} = E^n_\alpha - \frac{\Delta t}{2}\partial_\gamma H^n_\beta + \frac{\Delta t}{2}\partial_\beta H^{n+\frac{1}{2}}_{\gamma,k+1} - \left(\frac{\Delta t}{2}\right)^2\partial_{\alpha,\gamma}E^{n+\frac{1}{2}}_{\gamma,k+1},$$

$$H^{n+1}_{\beta,k+1} = H^n_\beta - \Delta t\partial_\gamma\frac{E^{n+1}_{\alpha,k+1} + E^n_\alpha}{2} + \Delta t\partial_\alpha E^{n+\frac{1}{2}}_{\gamma,k+1}.$$

References

[1] I. Ahmed, Z. Chen, Error reduced ADI-FDTD methods, IEEE Antennas Wireless Prop. Lett. 4 (2005) 323–325.
[2] Z. Chen, J. Zhang, An unconditionally stable 3-D ADI-MRTD method free of the CFL stability condition, IEEE Microwave Wireless Comp. Lett. 11 (2001) 49–351.
[3] M. Darms, R. Schuhmann, H. Spachmann, T. Weiland, Dispersion and asymmetry effects of ADI-FDTD, IEEE Microwave and Wireless Gomp Lett. 12 (2002) 491–493.
[4] B. Fornberg, A short proof of the unconditional stability of the ADI-FDTD scheme, University of Colorado, Department of Applied Mathematics, Technical Report 472, 2001.
[5] B. Fornberg, Some numerical techniques for Maxwell's equations in different types of geometries, in: Topics in Computational Wave Propagation 2002, Springer-Verlag, 2003, pp. 265–299.
[6] B. Fornberg, J. Zuev, J. Lee, Extrapolation methods for solving wave equations, preprint, 2005.
[7] W. Fu, E.L. Tan, A compact higher-order ADI-FDTD method, Microwave Opt. Technol. Lett. 44 (2005) 273–275.
[8] S.G. Garcia, T.-W. Lee, S.C. Hagness, On the accuracy of the ADI-FDTD method, IEEE Antennas Wireless Prop. Lett. 1 (2002) 31–34 (see also erratum p. 219).
[9] J. Lee, B. Fornberg, A split step approach for the 3-D Maxwell's equations in JCAM 158 (2003) 485–505.
[10] J. Lee, B. Fornberg, Some unconditionally stable time stepping methods for the 3D Maxwell's equations, J. Comput. Appl. Math. 166 (2004) 497–523.
[11] M.S. Min, C.H. Teng, The instability of the Yee scheme for the "Magic Time Step", J. Comput. Phys. 166 (2001) 418–424.
[12] T. Namiki, 3-D ADI-FDTD method-unconditionally stable time-domain algorithm for solving full vector Maxwell's equations, IEEE Trans. Microwave Theory Tech. 48 (October) (2000) 1743–1748.
[13] K.L. Schlager, J.B. Schneider, Comparison of the dispersion properties of several low-dispersion finite-difference time-domain algorithms, IEEE Trans. Antennas Propagat. 51 (March) (2003) 642–653.
[14] G. Sun, C.W. Truman, Some fundamental characteristics of the one-dimensional alternate-direction-implicit finite-difference time-domain method, IEEE Trans. Microwave Theory Tech. 52 (January) (2004) 46–52.
[15] G. Sun, C.W. Truman, A simple method to determine the time-step size to achieve a desired dispersion accuracy in ADI-FDTD, Microwave Opt. Technol. Lett 40 (2004) 487–490.
[16] A. Taflove, S. Hagness, Computational Electromagnetics – The Finite Difference Time-Domain Method, second ed., Artech House, Boston, MA, 2000.

[17] Z. Wang, J. Chen, Y. Chen, Development of a higher-order ADI-FDTD method, Microwave Opt. Technol. Lett 37 (2003) 8–12.
[18] S. Wang, J. Chen, Pre-iterative ADI-FDTD method for conductive medium, IEEE Trans. Microwave Theory Tech. 53 (June) (2005) 1913–1918.
[19] S. Wang, F. Teixeira, J. Chen, An iterative ADI-FDTD with reduced splitting error, IEEE Microwave Wireless Comp. Lett. 15 (2005) 1531–1533.
[20] X. Xie, Fast multiresolution methods in frequency and time domains for radiation and EMC applications, Ph.D. Dissertation, Arizona State University, 2005.
[21] K.S. Yee, Numerical solution of initial boundary value problems involving Maxwell's equations in isotropic media, IEEE Trans. Antennas Propagat. AP-14 (May) (1966) 302–307.
[22] A. Yefet, P.G. Petropoulos, A non-dissipative staggered fourth-order accurate explicit finite difference scheme for the time-domain Maxwell's equations, NASA ICASE 99-30, 1999.
[23] A. Yefet, E. Turkel, Fourth-order compact implicit method for the Maxwell equations with discontinuous coefficients, Appl. Numer. Math. 33 (2000) 125–134.
[24] A.P. Zhao, The influence of the time step on the numerical dispersion error of an unconditionally stable 3-D ADI-FDTD method: a simple and unified approach to determine the maximum allowable time step required by a desired numerical dispersion accuracy, Microwave Opt. Technol. Lett. 35 (2002) 60–65.
[25] A.P. Zhao, Consistency of the numerical dispersion relation expressed in different forms for the ADI-FDTD method, Microwave Opt. Technol. Lett 40 (2004) 12–13.
[26] F. Zheng, Z. Chen, J. Zhang, Toward the development of a three-dimensional unconditionally stable finite-difference time-domain method, IEEE Trans. Microwave Theory Tech. 48 (September) (2000) 1550–1558.